Optimal Detector with Correlated RF Source Signal in Ambient Backscatter Communication Systems

Anuranjan Jha, Vidhi Desai, Adarsh Patel
School of Computing and Electrical Engineering (SCEE), Indian Institute of Technology Mandi, H.P. India
Email: d20008@students.iitmandi.ac.in, b18168@students.iitmandi.ac.in, adarsh@iitmandi.ac.in

***Abstract*—This paper considers an ambient backscatter communication (AmBC) system with a generalized ambient radio frequency (RF) source signal, i.e., allowing correlated ambient RF source signal samples. A Neyman-Pearson (NP) criterion based optimal detector statistic for a correlated RF source signal in the AmBC system is obtained. To further analyze the detection performance of the proposed optimal detector, closed-form expressions of the probability of detection and probability of false alarm are derived. Simulation comparisons illustrate the proposed optimal detector's superior receiver operating characteristics (ROC) performance over the state-of-the-art detectors under the considered framework. Further, the simulation section demonstrates the ROC equivalence of the simulation performance with the derived analytical expressions of the proposed detector.**

***Index Terms*—Ambient backscatter communication (AmBC), Neyman-Pearson (NP), correlated signal.**

I. Introduction

Next-generation/ 6th-generation (6G) wireless standards envision to have a seamless and ubiquitous connectivity between the devices to support 4K video streaming, extended reality, cloud computing, etc. Also, the Internet of Everything (IoE) and broadband services use many low-power devices that transmit intermittently [1]. Billions of low-cost, sensor-type IoE connections are expected worldwide [2] for applications such as smart cities, smart home systems, environmental monitoring, and connected healthcare [3], [4]. Ambient backscatter communication (AmBC) system holds the potential to revolutionize the IoE [5]. AmBC system is an emerging wireless technology that allows low-power devices [5]–[7] to communicate by reflecting or absorbing the ambient radio-frequency (RF) signals, such as cellular signals, TV radio, and Wi-Fi [8], [9]. AmBC has the potential to transform how we perceive and utilize IoE devices, enabling low-power communication and increased spectrum utilization efficiency, inspiring a new era of innovation and sustainability.

AmBC systems offer an eco-friendly and sustainable solution for wireless communication in IoE applications [10], [11]. However, this increased lifetime of the IoE devices and efficient RF utilization comes at the cost of advanced signal processing techniques to detect the weak backscatter signals in AmBC systems, which is challenging considering a low signal-to-noise ratio, interference, and fading [12]. Several research studies [10]–[16], etc., have explored techniques to improve signal detection performance for various AmBC applications in this context. The authors of [13] demonstrated a working prototype for the AmBC system for small sensing devices, detecting signals using the instantaneous power of the received signal. The simple implementation of the energy detectors (ED) makes it a natural choice for adoption. For instance, the works [10], [14] employ passband ED at the reader for signal detection across varying numbers of RF source signal samples, whereas [15]–[17] apply ED for uplink detection in AmBC systems. Similarly, [16] considers RF signals and proposes optimal and sub-optimal ED detectors with different system settings. The works using ED [10], [11], [13]–[16], a simple-to-implement detector, suffers from an inferior detection performance in the low-signal or high interference/ noise power regimes, lead to SNR wall and related problems [18], [19].

Some associated studies have proposed variations of the ED [20], such as a maximum a posterior (MAP) based ED for the Internet of Things (IoT) in green communication paradigms [10], and a joint-ED for batteryless communication in IoT [11]. The authors in [21] modified a maximum likelihood (ML) technique which, upon further solving, results in ED. There are a few related studies that have explored alternative detection methods. For instance, authors in [22] investigated the magnitude detector (MD) in AmBC systems, a particular case of an improved energy detector (IED). The eigenvalue-based detector in [23] utilizes the maximum eigenvalue of the received signal covariance matrix at the backscatter receiver in the AmBC systems. Some learning-based detection techniques employ Support Vector Machine (SVM) and Random Forest [24], k-Nearest Neighbors (kNN) [25] but require a large training data. The RF signals from different cellular towers or Wi-Fi routers often exhibit statistical dependence. The above works predominantly consider scenarios with independent RF source samples, often neglecting any correlation [26]–[30]. The authors in [26] consider two spatially separated sensor nodes in a wireless sensor network (WSN) that observe correlated source samples. Similarly, the works [27]–[30] propose parameter estimation, joint transmission, efficient communication strategies and Blind source separation (BSS) while exploiting correlation in the source samples.

Hence this work presents a framework for realistic ambient RF source samples, i.e., consider correlated RF signal samples. The main contributions of the paper are as follows:

- An optimal detector statistic with correlated RF source samples using the Neyman-Pearson (NP) criterion is presented for the AmBC systems.
- Closed-form expressions for the probabilities of false

alarm (P_{FA}) and detection probability (P_D) are derived to analytically characterize the detection performance.
- ROC simulation plots demonstrates a consistent detection performance of the proposed detector over state-of-the-art (SOTA) detectors. The derived analytical results validates the superior performance of the proposed detector and match their simulation counterparts.

Section II presents the AmBC framework, and Sections III and IV present the optimal detection strategy and performance characteristics. Finally, Section V presents simulation results, and conclusions are presented in Section VI. This work uses bold font capital letters representing a matrix, such as $\mathbf{A}$. A bold font small letter, such as $\mathbf{a}$, denotes a vector. Regular lowercase letters are used to represent scalars. The Hermitian, determinant, and inverse of a matrix $\mathbf{A}$ are represented as $\mathbf{A}^H$, $\det(\mathbf{A})$, and $\mathbf{A}^{-1}$, respectively. A complex Gaussian distribution with a mean μ and variance σ^2 is denoted as $\mathcal{CN}(\mu, \sigma^2)$. The expectation of a random variable is denoted by $\mathbb{E}[\cdot]$ and $Pr(\cdot)$ for probability.

II. AmBC System Model

Fig. 1 illustrates an Ambient Backscatter Communication (AmBC) system that includes a tag/backscatter transmitter, a reader/backscatter receiver, and an ambient RF source. Each component is equipped with a single transmit/receive antenna. The RF source broadcasts the RF signal $s[n]$ at time n to a legacy receiver/user. The tag listens for the broadcast RF signal and adjusts its antenna impedance to modulate and reflect the RF source signal back to the reader [13], [14]. Let the vector $\mathbf{s}$ represent the concatenation of the RF signal over N time samples, defined for $1 \leq n \leq N$ as $\mathbf{s} = [s[1] \cdots s[n] \cdots s[N]]^T \in \mathbb{C}^{N\times 1}$. The RF signal vector $\mathbf{s}$ follows a complex Normal distribution with covariance matrix $\mathbf{C_s}$, expressed as $\mathbf{s} \sim \mathcal{CN}(\mathbf{0}, \mathbf{C_s})$, common in practical ambient sources like TV towers, Wi-Fi, and cellular signals [26]. The flat Rayleigh-faded wireless channel coefficients between the RF source and the reader, the RF source and the tag, and the tag and the reader are denoted as h_{sr}, h_{st}, and h_{tr}, respectively. The channel coefficients are assumed to be known to the reader and follows a complex Normal distribution with zero mean and unit variance. The signal vector $\mathbf{x} \in \mathbb{C}^{N\times 1}$ received at the tag, corresponding to the transmission of the RF signal vector $\mathbf{s}$, is given by

$$\mathbf{x} = h_{st}\mathbf{s}, \tag{1}$$

which is modulated and sent to the reader. Let ζ denote the scattering efficiency of the tag, and let the transmit symbol d take values from the set $d \in \{0, 1\}$, where $d = 1$ indicates reflection and $d = 0$ indicates no reflection. The data rate of the tag is assumed to be N times that of the RF source. The equivalent reflected tag signal $\mathbf{x}_b$, corresponding to the RF source signal in equation (1), is obtained as

$$\mathbf{x}_b = \zeta d\mathbf{x}. \tag{2}$$

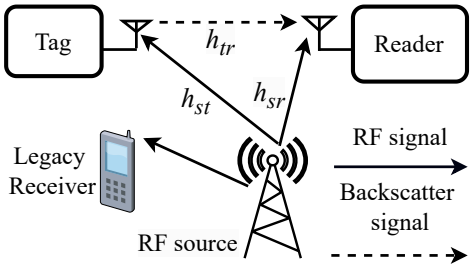

Fig. 1. Ambient Backscatter Communication (AmBC) System with an ambient RF source, a tag, a reader, and a legacy receiver.

The reader signal vector $\mathbf{y} \in \mathbb{C}^{N\times 1}$ corresponding to the transmission of the backscatter signal $\mathbf{x}_b$ in (2) from the tag and the RF source signal $\mathbf{s}$, is obtained as

$$\mathbf{y} = h_{sr}\mathbf{s} + h_{tr}\mathbf{x}_b + \mathbf{w}. \tag{3}$$

The additive noise vector $\mathbf{w} \in \mathbb{C}^{N\times 1}$, follows a complex Normal distribution, i.e., $\mathbf{w} \sim \mathcal{CN}(\mathbf{0}, \sigma^2\mathbf{I}_N)$, where $\mathbf{I}_N$ is an identity matrix of size $N \times N$. Using (2) and (3), the equivalent system model corresponding to the transmission of backscatter signal and RF source signal in AmBC is given as

$$\mathbf{y} = h_{sr}\mathbf{s} + h_{tr}\zeta d h_{st}\mathbf{s} + \mathbf{w}. \tag{4}$$

where the tag signal d takes binary values with equal probability. The optimal detector for the AmBC system in (4) is presented next.

III. Optimal Detector in the AmBC

The detection problem of the AmBC system described in (4) can be formulated as a binary decision problem, where $\mathcal{H}_0$ and $\mathcal{H}_1$ represent the null hypothesis and alternative hypothesis, respectively, corresponding to the tag signal transmission states $d = 0$ and $d = 1$. The received signal $\mathbf{y}$ at the reader for the transmission of the binary symbols $d \in \{0, 1\}$ is expressed as

$$\mathbf{y} = \begin{cases} h_0\mathbf{s} + \mathbf{w}; & \mathcal{H}_0 \\ h_1\mathbf{s} + \mathbf{w}; & \mathcal{H}_1 \end{cases}. \tag{5}$$

where $h_0 = h_{sr}$ and $h_1 = h_{sr} + \zeta h_{tr} h_{st}$.

Theorem III.1. *The NP-based optimal detection statistic $T_o(\mathbf{y})$ for the PDFs $p(\mathbf{y}|\mathcal{H}_0)$ in (8) and $p(\mathbf{y}|\mathcal{H}_1)$ in (9) for the correlated RF source signal in the AmBC system is*

$$T_o(\mathbf{y}) = \frac{1}{\sigma^6}\mathbf{y}^H \left[\mathbf{X}_1 - \mathbf{X}_0\right]\mathbf{y} \underset{\mathcal{H}_0}{\overset{\mathcal{H}_1}{\gtrless}} \gamma', \tag{6}$$

where γ' is the decision threshold defined as $\gamma' = \ln(\gamma'') + \ln(\det(\mathbf{C}_{\mathbf{y}|1})) - \ln(\det(\mathbf{C}_{\mathbf{y}|0}))$, γ'' is decision threshold, and $\mathbf{X}_i = \left(\mathbf{I}_N + (\sigma^2/|h_i|^2)\mathbf{C}_\mathbf{s}^{-1}\right)^{-1}$ for $i \in \{0, 1\}$.

Proof. The distributions of the received signal $\mathbf{y}$ in (5) corresponding to the two hypotheses be obtained as

$$\mathbf{y} \sim \begin{cases} \mathcal{CN}(\mathbf{0}, |h_0|^2\mathbf{C_s} + \sigma^2\mathbf{I}_N); & \mathcal{H}_0 \\ \mathcal{CN}(\mathbf{0}, |h_1|^2\mathbf{C_s} + \sigma^2\mathbf{I}_N); & \mathcal{H}_1 \end{cases}. \tag{7}$$

The above conditional PDFs when considering $\mathbf{C}_{\mathbf{y}|i} = |h_i|^2 \mathbf{C}_\mathbf{s} + \sigma^2 \mathbf{I}_N$ for $i \in \{0,1\}$, reduces to

$$p(\mathbf{y}|\mathcal{H}_0) \sim \mathcal{CN}(\mathbf{0}, \mathbf{C}_{\mathbf{y}|0}) \tag{8}$$
$$p(\mathbf{y}|\mathcal{H}_1) \sim \mathcal{CN}(\mathbf{0}, \mathbf{C}_{\mathbf{y}|1}), \tag{9}$$

where $p(\mathbf{y}|\mathcal{H}_i)$ is the conditional PDFs of $\mathbf{y}$ corresponding to hypothesis $\mathcal{H}_i$ for $i \in \{0,1\}$. Given the conditional PDFs of $\mathbf{y}$ in (7), the NP based optimal log-likelihood ratio (LLR) test $\mathcal{L}(\mathbf{y})$ can be expressed as

$$\mathcal{L}(\mathbf{y}) = \ln\left(\frac{p(\mathbf{y}|\mathcal{H}_1)}{p(\mathbf{y}|\mathcal{H}_0)}\right) \underset{\mathcal{H}_0}{\overset{\mathcal{H}_1}{\gtrless}} \ln\gamma''. \tag{10}$$

The conditional PDFs $p(\mathbf{y}|\mathcal{H}_i)$ for $i \in \{0,1\}$ in (8) and (9) is defined [31] as

$$p(\mathbf{y}|\mathcal{H}_i) = \frac{1}{\pi^N \det(\mathbf{C}_{\mathbf{y}|i})} \exp\left\{-\mathbf{y}^H \mathbf{C}_{\mathbf{y}|i}^{-1} \mathbf{y}\right\}. \tag{11}$$

Matrix inversion lemma [31] is used to further simplify $\mathbf{C}_{\mathbf{y}|i}^{-1}$ in (11) to (12).

$$\begin{aligned}\mathbf{C}_{\mathbf{y}|i}^{-1} &= (\sigma^2 \mathbf{I}_N + |h_i|^2 \mathbf{C}_\mathbf{s})^{-1} \\ &= \frac{1}{\sigma^2}\mathbf{I}_N - \frac{1}{\sigma^6}\mathbf{X}_i,\end{aligned} \tag{12}$$

where $\mathbf{X}_i = \left(\mathbf{I}_N + (\sigma^2/|h_i|^2)\mathbf{C}_\mathbf{s}^{-1}\right)^{-1}$ for $i \in \{0,1\}$. Using the PDFs $p(\mathbf{y}|\mathcal{H}_i)$ for $i \in \{0,1\}$ and $\mathbf{X}_i$ in the LLR (10) will yield the detection statistic (6) in Theorem III.1. □

The next section characterizes the detection performance of the optimal detector statistic presented in Theorem III.1.

IV. Performance Analysis of the Proposed Optimal Detector

This section derives the detection performance of the proposed text in (6) upon obtaining its conditional PDF. The detection statistic at the reader is further simplified to obtain tractable conditional PDFs of the detection statistic corresponding to the two hypotheses. Let the singular value decomposition of RF source signal covariance matrix $\mathbf{C}_\mathbf{s}$ be $\mathbf{C}_\mathbf{s} = \mathbf{U}\mathbf{\Sigma}\mathbf{U}^H$, where $\mathbf{U} \in \mathbb{C}^{N\times N}$ is a unitary matrix and the diagonal matrix $\mathbf{\Sigma}$ contains singular values $\sigma_1, \cdots, \sigma_n, \cdots, \sigma_N$ at its principle diagonal with $\sigma_{n-1} \geq \sigma_n > 0$, for $1 < n \leq N$. The $\mathbf{X}_i$ in (12) is simplified as

$$\begin{aligned}\mathbf{X}_i &= \left(\mathbf{I}_N + (\sigma^2/|h_i|^2)\mathbf{C}_\mathbf{s}^{-1}\right)^{-1} \\ &= \left(\mathbf{I}_N + (\sigma^2/|h_i|^2)(\mathbf{U}\mathbf{\Sigma}\mathbf{U}^H)^{-1}\right)^{-1} \qquad (13) \\ &= \left(\mathbf{I}_N + (\sigma^2/|h_i|^2)\mathbf{U}\mathbf{\Sigma}^{-1}\mathbf{U}^H\right)^{-1} \\ &= \left(\mathbf{U}\left(\mathbf{I}_N + (\sigma^2/|h_i|^2)\mathbf{\Sigma}^{-1}\right)\mathbf{U}^H\right)^{-1} \\ &= \mathbf{U}\left(\mathbf{I}_N + (\sigma^2/|h_i|^2)\mathbf{\Sigma}^{-1}\right)^{-1}\mathbf{U}^H, \qquad (14)\end{aligned}$$

where (13) follows by using the decomposition of $\mathbf{C}_\mathbf{s}$ and further solving gives (14). For $\mathbf{X}_i$ in (14), $\mathbf{X}_1 - \mathbf{X}_0 = \mathbf{U}\mathbf{\Lambda}\mathbf{U}^H$ such that the diagonal matrix $\mathbf{\Lambda}$, defined in (15), contains the singular values λ_n, given in (16), at its principal diagonal with $\lambda_{n-1} \geq \lambda_n$ for $1 < n \leq N$ as

$$\mathbf{\Lambda} = \left(\mathbf{I}_N + \frac{\sigma^2}{|h_1|^2}\mathbf{\Sigma}^{-1}\right)^{-1} - \left(\mathbf{I}_N + \frac{\sigma^2}{|h_0|^2}\mathbf{\Sigma}^{-1}\right)^{-1} \tag{15}$$

$$\lambda_n = \frac{1}{1+|h_1|^2\frac{\sigma^2}{\sigma_n}} - \frac{1}{1+|h_0|^2\frac{\sigma^2}{\sigma_n}}, \quad n = 1,2,\cdots,N. \tag{16}$$

The entries of the diagonal matrix $\mathbf{\Lambda}$ are assumed to be non-negative, i.e., $\lambda_n \geq 0$, $\forall n$ in (16), which holds when $|h_1|^2 \geq |h_0|^2$. Using the simplified form of $\mathbf{X}_1 - \mathbf{X}_0$, the detection statistic equivalently reduces to

$$T_o(\mathbf{y}) \doteq \mathbf{y}^H(\mathbf{X}_1 - \mathbf{X}_0)\mathbf{y} \tag{17}$$
$$= \mathbf{y}^H\mathbf{U}\mathbf{\Lambda}\mathbf{U}^H\mathbf{y} \tag{18}$$
$$T_o(\tilde{\mathbf{y}}) = \tilde{\mathbf{y}}^H\mathbf{\Lambda}\tilde{\mathbf{y}}$$
$$= \sum_{n=1}^{N}\lambda_n|\tilde{y}_n|^2 \underset{\mathcal{H}_0}{\overset{\mathcal{H}_1}{\gtrless}} \gamma, \tag{19}$$

where the symbol $\doteq$ in (17) shows the equivalence upto scaling, and (18) follows from the substitution mentioned earlier, (19) is obtained by $\tilde{\mathbf{y}} = \mathbf{U}^H\mathbf{y} = [\tilde{y}_1, \cdots, \tilde{y}_N]^T \in \mathbb{C}^{N\times 1}$, and threshold γ from $\gamma = \sigma^6\gamma'$. The PDFs of $\mathbf{y}$ in (7) using the transformation $\tilde{\mathbf{y}} = \mathbf{U}^H\mathbf{y}$ corresponding to the two hypotheses reduces to

$$p(\tilde{\mathbf{y}}|\mathcal{H}_i) \sim \mathcal{CN}(\mathbf{0}, |h_i|^2\mathbf{\Sigma} + \sigma^2\mathbf{I}_N), \quad \text{for } i \in \{0,1\}. \tag{20}$$

Therefore the element n of the vector $\tilde{\mathbf{y}}$, i.e., $\tilde{y}_n$ follows a complex Normal PDF $p(\tilde{y}_n|\mathcal{H}_i) \sim \mathcal{CN}(0, \tilde{\sigma}_{n|i}^2)$ where $\tilde{\sigma}_{n|i}^2 = |h_i|^2\lambda_n + \sigma^2$. Let $a_{n|i} = \frac{\tilde{y}_n}{\tilde{\sigma}_{n|i}}$ for $i \in \{0,1\}$, i.e., $p(a_{n|i}|\mathcal{H}_i) \sim \mathcal{CN}(0,1)$. Using the PDFs presented above, the probabilities of false alarm and detection are presented in the Lemma IV.1 below.

Lemma IV.1. *The false alarm (P_{FA}) and probabilities of detection (P_D) for the correlated RF source signal-based optimal detection statistic in* (6) *for the AmBC system are given as*

$$P_{FA} = \textstyle\sum_{n=1}^{N} A_n \exp\left(\frac{-\gamma}{2\alpha_n}\right) \tag{21}$$
$$P_D = \textstyle\sum_{n=1}^{N} B_n \exp\left(\frac{-\gamma}{2\beta_n}\right), \tag{22}$$

where the constants A_n and B_n are defined as $A_n = \prod_{l=1,l\neq n}^{N}\frac{1}{1-\alpha_l/\alpha_n}$ and $B_n = \prod_{l=1,l\neq n}^{N}\frac{1}{1-\beta_l/\beta_n}$, with $\alpha_n = \lambda_n\tilde{\sigma}_{n|0}^2$ and $\beta_n = \lambda_n\tilde{\sigma}_{n|1}^2$.

Proof. The proof for the two probabilities are given in the following two subsections.

A. Probability of False Alarm (P_{FA})

The probability of false alarm refers to the probability of decoding a symbol as 1 (reflect the RF source signal) when the transmitted symbol was 0 (absorb the RF source signal), i.e., to decide in favor of alternative hypothesis $\mathcal{H}_1$ when the

null hypothesis $\mathcal{H}_0$ occurred. As defined next in (23) and is further solved as

$$P_{FA} = Pr\left\{T_o(\tilde{\mathbf{y}}) > \gamma; \mathcal{H}_0\right\} \tag{23}$$

$$= Pr\left\{\sum_{n=1}^{N} \lambda_n \left|\tilde{y}_n\right|^2 > \gamma; \mathcal{H}_0\right\} \tag{24}$$

$$= Pr\left\{\sum_{n=1}^{N} \alpha_n |a_{n|0}|^2 > \gamma\right\} \tag{25}$$

$$= \int_{\gamma}^{\infty} p_T(t)\ dt, \tag{26}$$

where (24) is obtained from (19), (25) is obtained using $\alpha_n = \lambda_n \tilde{\sigma}^2_{n|0}$, $a_{n|0} = \frac{\tilde{y}_n}{\tilde{\sigma}_{n|0}}$. Observe $a_{n|0} \sim \mathcal{CN}(0,1)$ and hence $|a_{n|0}|^2$ follows a Chi-squared PDF with two degrees of freedom, i.e., $|a_{n|0}|^2 \sim \chi^2_2$. Also, $p_T(t)$ in (26) denotes the probability density function of the test $T_o(\tilde{\mathbf{y}})$ corresponding to the null hypothesis, defined next in (27) as

$$p_T(t) = \begin{cases} \frac{1}{2\pi}\int_{-\infty}^{\infty} \phi_T(\omega) e^{-j\omega t} d\omega & t \geq 0 \\ 0 & t < 0 \end{cases}, \tag{27}$$

where $\phi_T(\omega)$ denotes the characteristic function of the test statistic $T_o(\tilde{\mathbf{y}})$ corresponding to the null hypothesis [31], [32] and is derived next

$$\phi_T(\omega) = \mathbb{E}\Big\{ \exp\left(j\omega T_o(\tilde{\mathbf{y}})\right) \Big\} = \mathbb{E}\Big\{ \exp\left(j\omega \sum_{n=1}^{N} \alpha_n |a_{n|0}|^2\right) \Big\}$$

$$= \prod_{n=1}^{N} \mathbb{E}\Big\{ \exp\left(j\omega\alpha_n |a_{n|0}|^2\right) \Big\} \tag{28}$$

$$= \prod_{n=1}^{N} \frac{1}{1 - 2j\alpha_n\omega} \tag{29}$$

$$= \sum_{n=1}^{N} \frac{A_n}{1 - 2j\alpha_n\omega}. \tag{30}$$

Using the independence, the summation of N term is converted to the product of N term to get (28). Use $|a_{n|0}|^2 \sim \chi^2_2$ in the the characteristic function to get (29), and use the partial fraction [31] to obtain (30) where

$$A_n = \prod_{l=1, l\neq n}^{N} \frac{1}{1 - \alpha_l/\alpha_n}. \tag{31}$$

Using the PDF $p_T(t)$ in (27) for the test $T_o(\tilde{\mathbf{y}}), t \geq 0$ and the characteristic function in $\phi_T(\omega)$ (30), the probability of false alarm (P_{FA}) defined in (26) is simplified to

$$P_{FA} = \int_{\gamma}^{\infty} p_T(t)\ dt$$

$$= \int_{\gamma}^{\infty} \frac{1}{2\pi} \int_{-\infty}^{\infty} \sum_{n=1}^{N} \frac{A_n}{1 - 2j\alpha_n\omega} e^{-j\omega t} d\omega\ dt$$

$$= \int_{\gamma}^{\infty} \sum_{n=1}^{N} \frac{1}{2\pi} \int_{-\infty}^{\infty} \frac{A_n}{1 - 2j\alpha_n\omega} e^{-j\omega t} d\omega\ dt \tag{32}$$

where (32) is obtained on interchanging the order of the summation and integration, and is further simplified as

$$P_{FA} = \int_{\gamma}^{\infty} \sum_{n=1}^{N} \mathcal{F}^{-1}_{-t}\left\{\frac{A_n}{1 - 2j\alpha_n\omega}\right\} dt$$

$$= \int_{\gamma}^{\infty} \sum_{n=1}^{N} \frac{1}{2\alpha_n} A_n \exp\left(\frac{-t}{2\alpha_n}\right) dt \tag{33}$$

$$= \sum_{n=1}^{N} \frac{1}{2\alpha_n} A_n \int_{\gamma}^{\infty} \exp\left(\frac{-t}{2\alpha_n}\right) dt$$

$$P_{FA} = \sum_{n=1}^{N} A_n \exp\left(\frac{-\gamma}{2\alpha_n}\right).$$

where (33) is obtained on taking the inverse Fourier transform $(\mathcal{F}^{-1}_{-t})$. Hence, the probability of false alarm P_{FA} for the optimal test statistic in (6) corresponding to the null hypothesis $\mathcal{H}_0$ is derived in (21).

B. Probability of Detection

The probability of detection (P_D) in (34) refers to the probability of deciding in favor of alternative hypothesis $\mathcal{H}_1$ when the alternative hypothesis $\mathcal{H}_1$ occurred. The proof for the P_D in (22) can be obtained along similar lines as the proof of the P_{FA} in (21). An outline of the same is presented next

$$P_D = Pr\left\{T_o(\tilde{\mathbf{y}}) > \gamma; \mathcal{H}_1\right\} \tag{34}$$

$$= Pr\left\{\sum_{n=1}^{N} \lambda_n \left|\tilde{y}_n\right|^2 > \gamma; \mathcal{H}_1\right\} \tag{35}$$

$$= Pr\left\{\sum_{n=1}^{N} \beta_n |a_{n|1}|^2 > \gamma\right\} \tag{36}$$

$$= \int_{\gamma}^{\infty} p_T(t)\ dt, \tag{37}$$

where (35) is obtained from (19), (36) is obtained using $\beta_n = \lambda_n \tilde{\sigma}^2_{n|1}$ and $a_{n|1} = \frac{\tilde{y}_n}{\tilde{\sigma}_{n|1}}$. Observe $a_{n|1} = \frac{\tilde{y}_n}{\tilde{\sigma}_{n|1}} \sim \mathcal{CN}(0,1)$ and hence $|a_{n|1}|^2$ follows a Chi-squared PDF with two degrees of freedom, i.e., $|a_{n|1}|^2 \sim \chi^2_2$. The PDF $p_T(t)$ of the test statistic $T_o(\tilde{\mathbf{y}})$ corresponding to $\mathcal{H}_1$ is similar to the definition in (27) where $\phi_T(\omega)$ now denote the characteristic function of $T_o(\tilde{\mathbf{y}})$ corresponding to $\mathcal{H}_1$ [31], [32] and is derived to

$$\phi_T(\omega) = \sum_{n=1}^{N} \frac{B_n}{1 - 2j\beta_n\omega}, \tag{38}$$

where $B_n = \prod_{l=1, l\neq n}^{N} \frac{1}{1-\beta_l/\beta_n}$. The P_D defined in (37) be further simplified using (38) to get (22).

□

The following section presents the simulation analysis.

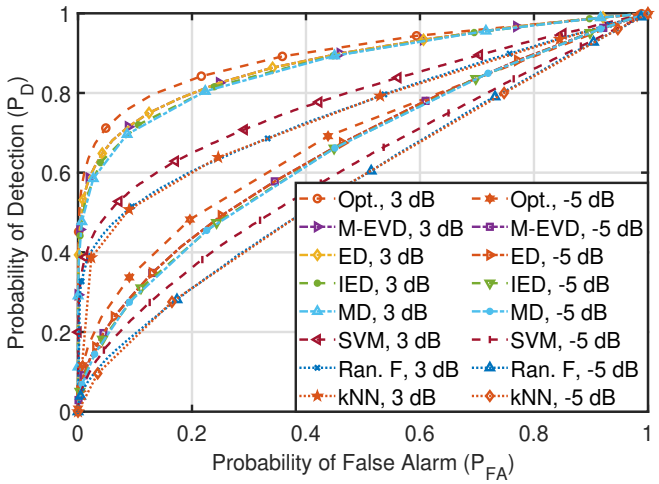

Fig. 2. ROC plots for the optimal detector (Opt.) statistic $T_o(\mathbf{y})$ in Theorem III.1, when compared with the ED [15], MD, IED [22], M-EVD [23], SVM, Random Forest (Ran. F) [24], and kNN [25] at SINR $\in \{-5, 3\}$ dB.

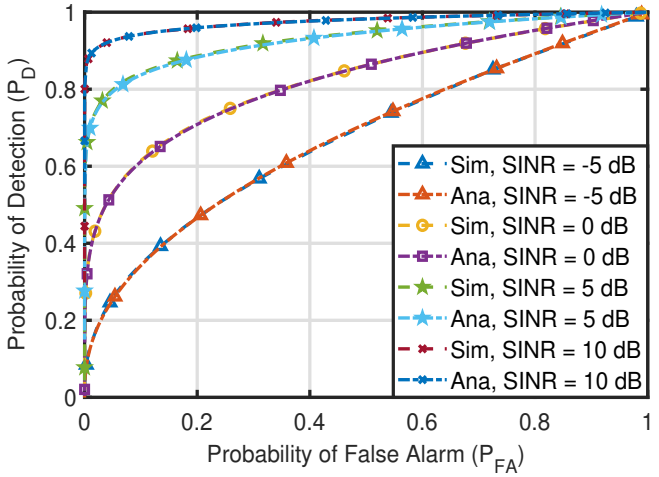

Fig. 3. ROC simulations (Sim) and the analytical (Ana) plots for the optimal detector statistic $T_o(\mathbf{y})$ presented in the Lemma III.1 at varying SINR $\in \{-5, 0, 5, 10\}$ dB.

V. Simulation Result

Consider an AmBC system in (4) where each of the channel gain factors h_{sr}, h_{st}, and h_{tr}, each follows a zero-mean complex Gaussian distribution with unit variance, known at the reader. Consequently, their magnitudes adhere to a Rayleigh distribution, realistically representing multipath effects in non-line-of-sight environments. The transmitted backscatter tag symbol $d \in \{0, 1\}$ assumes equiprobable binary values and RF source signal power (P_s), that contributes to interference. The RF source signal vector $\mathbf{s}$ follows a complex Normal distribution having zero mean and covariance matrix $\mathbf{C_s}$ expressed as $\mathbf{s} \sim \mathcal{CN}(\mathbf{0}, \mathbf{C_s})$. The covariance matrix, defined in (13), is given by $\mathbf{C_s} = \mathbf{U\Sigma U}^H$, where $\mathbf{U}$ is a unitary matrix. The entries of the diagonal matrix $\mathbf{\Sigma}$ are evenly spaced between 1 and N, and are appropriately normalized to (P_s). Unless specified otherwise, the transmission rate of the RF source signal is assumed to be twice that of the tag signal $(N = 2)$, and the reflection coefficient ζ is set to unity.

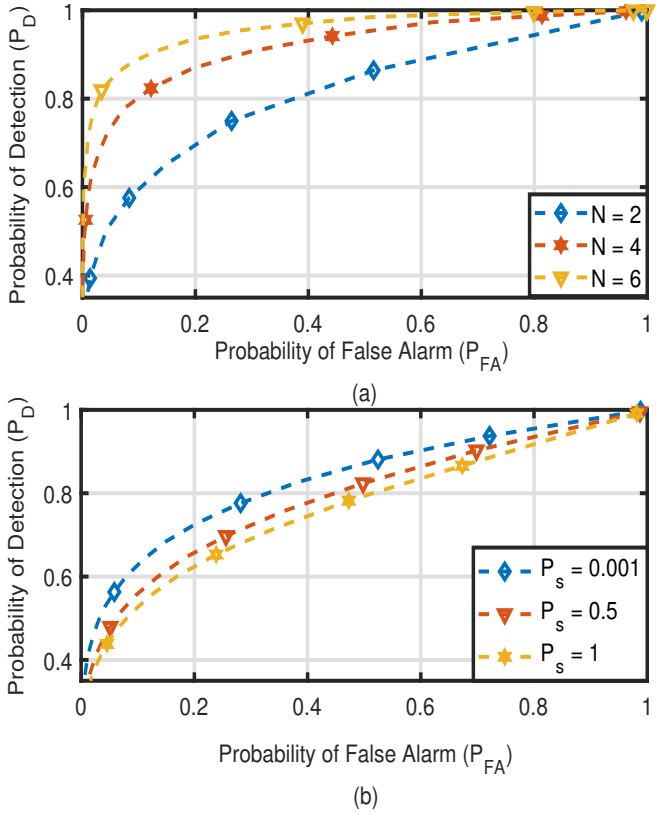

Fig. 4. ROC plots for the optimal detector statistic $T_o(\mathbf{y})$ in Theorem (III.1) at SINR = 0 dB at (a) different ratios of the data rates of the RF source to the tag signal, $N \in \{2, 4, 6\}$ with $P_s = 0.01$ watts (b) different $P_s \in \{0.001, 0.5, 1\}$ watts, and $N = 2$.

ROC comprehensively evaluates a detector across all decision thresholds, thus ROC comparisons are presented between the proposed detection statistic in (6) in Theorem III.1 and state-of-the-art methods: the magnitude-based detector (MD) [22], which computes the sum of the magnitude of the received signal $\mathbf{y}$ in (4); IED [22] sums their p-th powers; ED [15] analyzes the energy of the received signal; and the M-EVD [23] evaluates the maximum eigenvalue of the received signal's covariance matrix. Also, the learning-based approaches, like kNN [25] classify signals by comparing their similarity to known signals; SVM [24] finds the best boundary to separate signals, and Random Forest [24] uses an ensemble of decision trees for detection. However, the learning-based approaches are additionally required to train with the tag bit $d \in \{0, 1\}$ per SNR with 10^5 labeled samples.

Fig. 2 compares the ROC performance of the proposed optimal statistic detector in (6) with the ED, MD, and M-EVD at the varying levels of the signal strength ratio to interference plus noise (SINR) $\in \{-5, 3\}$ dB. The figure illustrates the superior performance of the proposed detector over the SOTA detectors. Also, the performance of the detectors is observed to improve with the increase in the SINR levels. Fig. 3 shows the ROC performance equivalence between the results obtained via simulation and the analytical probabilities derived in (21) and (22) for the proposed detectors at different SINR $\in \{-5, 0, 5, 10\}$ dB. Fig. 4 presents the P_D vs. P_{FA}

performance comparisons of the proposed detector statistic in Theorem III.1 at SINR $= 0$ dB for varying the ratios of the data rates of the RF source to the tag signal, (N) and $P_{\mathbf{s}}$. The P_D axis is limited to a range to highlight the relevant portion. Fig. 4(a) presents the ROC plot for $N \in \{2, 4, 6\}$. The detection performance of the introduced detector is readily observed to improve with an increase in the factor N. A similar trend in Fig. 4(b) for varying levels of $P_{\mathbf{s}} \in \{0.001, 0.5, 1\}$ watts is observed where the performance of the proposed detector improves with a decrease in $P_{\mathbf{s}}$.

VI. Conclusion

This work introduced a novel optimal detector with correlated RF source signals in AmBC systems. This approach expands upon existing frameworks found in the literature. The ROC comparisons in the simulation section demonstrated that the proposed detector outperformed state-of-the-art ED, along with the allied MD, M-EVD, IED, SVM, Random Forest, and kNN detectors. Additionally, the work derived closed-form expressions for P_D and P_{FA} within the framework of correlated RF source signals in the AmBC system. The results confirmed the ROC analysis, showing a strong agreement between the simulation outcomes and their analytical counterparts.

References

[1] M. Ahmed, M. Shahwar, F. Khan, W. Ullah Khan, A. Ihsan, U. Sadiq Khan, F. Xu, and S. Chatzinotas, "NOMA-Based Backscatter Communications: Fundamentals, Applications, and Advancements," *IEEE Internet of Things Journal*, vol. 11, no. 11, pp. 19303–19327, 2024.

[2] "CISCO Annual Internet Report 2018-2023."

[3] J. Xin and S. Xu, "Cellular Backscatter Communication: Ambient IoT Technology," in *2024 IEEE International Symposium on Broadband Multimedia Systems and Broadcasting (BMSB)*, pp. 1–6, 2024.

[4] X. Lu, Y. Yang, and W. Gong, "Challenges of ambient WiFi backscatter systems in healthcare applications," *Computer Networks*, vol. 251, p. 110608, 2024.

[5] C. Xu, L. Yang, and P. Zhang, "Practical Backscatter Communication Systems for Battery-Free Internet of Things: A Tutorial and Survey of Recent Research," *IEEE Signal Processing Magazine*, vol. 35, no. 5, pp. 16–27, 2018.

[6] S. Abdallah, A. I. Salameh, M. Saad, and M. A. Albreem, "Asynchronous Ambient Backscatter Communication Systems: Joint Timing Offset and Channel Estimation," *IEEE Transactions on Communications*, pp. 1–1, 2024.

[7] Y. Yang, Y. Feng, W. Gong, and Y. Yang, "Efficient LTE Backscatter with Uncontrolled Ambient Traffic," in *IEEE INFOCOM 2024 - IEEE Conference on Computer Communications*, pp. 1781–1790, 2024.

[8] N. Van Huynh, D. T. Hoang, X. Lu, D. Niyato, P. Wang, and D. I. Kim, "Ambient Backscatter Communications: A Contemporary Survey," *IEEE Communications Surveys Tutorials*, vol. 20, no. 4, pp. 2889–2922, 2018.

[9] A. Benoni, G. Oliveri, P. Rocca, M. Salucci, F. Zardi, and A. Massa, "Smart EM Environments: Current Trends and Future Perspectives," in *2022 16th European Conference on Antennas and Propagation (EuCAP)*, pp. 1–4, 2022.

[10] J. Wang, P. Ren, D. Xu, and L. Lu, "A Novel Signal Detection Method Based on Multivariate Test Statistics for Ambient Backscatter Communications," in *2022 IEEE/CIC International Conference on Communications in China (ICCC)*, pp. 713–718, 2022.

[11] J. Qian, F. Gao, G. Wang, S. Jin, and H. Zhu, "Noncoherent Detections for Ambient Backscatter System," *IEEE Transactions on Wireless Communications*, vol. 16, no. 3, pp. 1412–1422, 2017.

[12] F. Rezaei, C. Tellambura, and S. Herath, "Large-Scale Wireless-Powered Networks with Backscatter Communications—A Comprehensive Survey," *IEEE Open Journal of the Communications Society*, vol. 1, pp. 1100–1130, 2020.

[13] V. Liu, A. Parks, V. Talla, S. Gollakota, D. Wetherall, and J. R. Smith, "Ambient Backscatter: Wireless Communication Out of Thin Air," *ACM SIGCOMM computer communication review*, vol. 43, no. 4, pp. 39–50, 2013.

[14] G. Wang, F. Gao, R. Fan, and C. Tellambura, "Ambient Backscatter Communication Systems: Detection and Performance Analysis," *IEEE Transactions on Communications*, vol. 64, no. 11, pp. 4836–4846, 2016.

[15] J. K. Devineni and H. S. Dhillon, "Ambient Backscatter Systems: Exact Average Bit Error Rate Under Fading Channels," *IEEE Transactions on Green Communications and Networking*, vol. 3, no. 1, pp. 11–25, 2019.

[16] J. Qian, F. Gao, G. Wang, and S. Jin, "Symbol Detection and Performance Analysis of the Ambient Backscatter System," in *2016 IEEE/CIC International Conference on Communications in China (ICCC)*, pp. 1–6, 2016.

[17] K. Lu, G. Wang, F. Qu, and Z. Zhong, "Signal detection and BER analysis for RF-powered devices utilizing ambient backscatter," in *2015 International Conference on Wireless Communications Signal Processing (WCSP)*, pp. 1–5, 2015.

[18] A. Mariani, A. Giorgetti, and M. Chiani, "SNR Wall for Energy Detection with Noise Power Estimation," in *2011 IEEE International Conference on Communications (ICC)*, pp. 1–6, 2011.

[19] R. Tandra and A. Sahai, "SNR Walls for Signal Detection," *IEEE Journal of Selected Topics in Signal Processing*, vol. 2, no. 1, pp. 4–17, 2008.

[20] Q. Tao, C. Zhong, X. Chen, H. Lin, and Z. Zhang, "Optimal Detection for Ambient Backscatter Communication Systems With Multiantenna Reader Under Complex Gaussian Illuminator," *IEEE Internet of Things Journal*, vol. 7, no. 12, pp. 11371–11383, 2020.

[21] J. Qian, F. Gao, G. Wang, S. Jin, and H. Zhu, "Semi-Coherent Detection and Performance Analysis for Ambient Backscatter System," *IEEE Transactions on Communications*, vol. 65, no. 12, pp. 5266–5279, 2017.

[22] Y. Chen and W. Feng, "Novel Signal Detectors for Ambient Backscatter Communications in Internet of Things Applications," *IEEE Internet of Things Journal*, pp. 1–1, 2023.

[23] Q. Tao, C. Zhong, X. Chen, H. Lin, and Z. Zhang, "Maximum-eigenvalue detector for multiple antenna ambient backscatter communication systems," *IEEE Transactions on Vehicular Technology*, vol. 68, no. 12, pp. 12411–12415, 2019.

[24] Y. Hu, P. Wang, Z. Lin, M. Ding, and Y.-C. Liang, "Machine Learning Based Signal Detection for Ambient Backscatter Communications," in *ICC 2019 - 2019 IEEE International Conference on Communications (ICC)*, pp. 1–6, 2019.

[25] X. Wang, R. Duan, H. Yigitler, E. Menta, and R. Jantti, "Machine Learning-Assisted Detection for BPSK-Modulated Ambient Backscatter Communication Systems," in *2019 IEEE Global Communications Conference (GLOBECOM)*, pp. 1–6, 2019.

[26] Y. Dong, Z. Chen, J. Wang, and B. Shim, "Optimal Power Control for Transmitting Correlated Sources With Energy Harvesting Constraints," *IEEE Transactions on Wireless Communications*, vol. 17, no. 1, pp. 461–476, 2018.

[27] K. P. Rajput, M. F. Ahmed, N. K. D. Venkategowda, A. K. Jagannatham, G. Sharma, and L. Hanzo, "Robust Decentralized and Distributed Estimation of a Correlated Parameter Vector in MIMO-OFDM Wireless Sensor Networks," *IEEE Transactions on Communications*, vol. 69, no. 10, pp. 6894–6908, 2021.

[28] J. Garcia-Frias and Y. Zhao, "Near-Shannon/Slepian-wolf performance for unknown correlated sources over AWGN channels," *IEEE Transactions on Communications*, vol. 53, no. 4, pp. 555–559, 2005.

[29] A. Padakandla, "Communicating Correlated Sources Over MAC and Interference Channels I: Separation-Based Schemes," *IEEE Transactions on Information Theory*, vol. 66, no. 7, pp. 4104–4128, 2020.

[30] Y. Deville and S. Hosseini, "Blind source separation methods based on output nonlinear correlation for bilinear mixtures of an arbitrary number of possibly correlated signals," in *2020 IEEE 11th Sensor Array and Multichannel Signal Processing Workshop (SAM)*, pp. 1–5, 2020.

[31] S. M. Kay, "Fundamentals of Statistical Signal Processing, Volume 2: Detection Theory. 1998."

[32] A. Patel, S. Biswas, and A. K. Jagannatham, "Optimal GLRT-Based Robust Spectrum Sensing for MIMO Cognitive Radio Networks with CSI Uncertainty," *IEEE Transactions on Signal Processing*, vol. 64, no. 6, pp. 1621–1633, 2016.